Downward Wave Propagation on the Polar Vortex

R. K. SCOTT* AND D. G. DRITSCHEL

School of Mathematics, University of St Andrews, St Andrews, United Kingdom

(Manuscript received 9 April 2004, in final form 2 February 2005)

ABSTRACT

This paper considers the propagation of waves on the edge of a stratospheric polar vortex, represented by a three-dimensional patch of uniform potential vorticity in a compressible quasigeostrophic system. Waves are initialized by perturbing the vortex from axisymmetry in the center of the vortex, and their subsequent upward and downward propagation is measured in terms of a nonlinear, pseudomomentum-based wave activity. Under conditions typical of the winter stratosphere, the dominant direction of wave propagation is downward, and wave activity accumulates in the lower vortex levels. The reason for the preferred downward propagation arises from a recent result of Scott and Dritschel, which showed that the three-dimensional Green's function in the compressible system contains an anisotropy that causes a general differential rotation in a finite volume vortex. The sense of the differential rotation is to stabilize the upper vortex and destabilize the lower vortex. This mechanism is particularly interesting in view of recent interest in the downward influence of the stratosphere on the troposphere and also provides a possible conservative, balanced explanation of the formation of the robust dome plus annulus potential vorticity structure observed in the upper stratosphere.

1. Introduction

In a recent study, Scott and Dritschel (2005, hereafter SD) showed that the Green's function of the compressible quasigeostrophic system has an anisotropic decay, with a slower, algebraic decay vertically upward compared with a faster, exponential decay in all other directions. Here, compressible quasigeostrophic system refers to the atmospheric situation in which the background density is exponentially decreasing with height, and should be contrasted with the Boussinesq system, with constant background density, whose Green's function has an isotropic $1/r$ decay (in suitably scaled coordinates) in all directions. An important consequence of the anisotropic decay in the compressible system is that finite volume vortices exhibit a differential rotation in which the upper vortex rotates faster than the lower vortex. They went on to show that for general unstable, ellipsoidal vortices, the differential rotation leads to a stabilization of the upper vortex and a destabilization of the lower vortex, with the result that wave activity, or, equivalently, horizontal disturbances to the shape of the vortex boundary, propagates almost entirely downward. For the ellipsoidal vortices considered in that study, the downward propagation led to the violent destruction of the lower vortex layers, an example of which is shown in Fig. 1.

This paper considers the extent to which the results of SD are applicable to the particular situation of Rossby wave propagation on the edge of the winter stratospheric polar vortex. The subject of wave propagation and wave breaking is of fundamental importance to many processes in the middle atmosphere, determining both the local mixing of chemical species and the large-scale mean meridional circulation, with consequent implications for the thermal and chemical structure of the atmosphere (e.g., McIntyre 1990; Holton et al. 1995). Recent interest in the stratospheric influence on the troposphere (e.g., Baldwin and Dunkerton 2001, 1999; Thompson and Wallace 1998; Thompson et al. 2002) has also raised the possibility that downward propagating waves may provide an important dynamical link between the two regions (Perlwitz and Harnik 2003). In this paper we show that the mechanism for preferred downward propagation described in SD is a

* Current affiliation: NorthWest Research Associates, Inc., Bellevue, Washington.

Corresponding author address: R. K. Scott, NorthWest Research Associates, Inc., P.O. Box 3027, Bellevue, WA 98009-3027. E-mail: scott@nwra.com

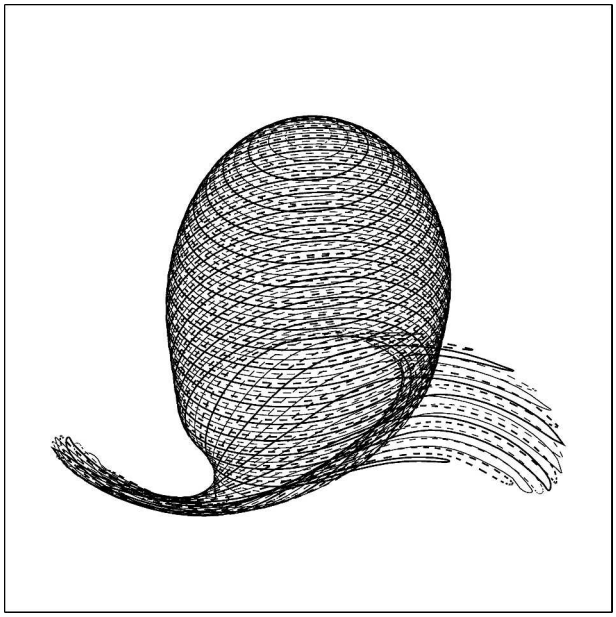

FIG. 1. Stage in the nonlinear evolution of an ellipsoid with semiaxis (a, b, c) of horizontal aspect ratio $a/b = 0.5$, vertical aspect ratio $c/\sqrt{ab} = 4/3$, and vertical extent $D \equiv 2c = 2H$, where H is the density-scale height, showing downward propagation of ellipticity and wave breaking in the lower vortex. From Scott and Dritschel (2005).

generic feature of flows typical of the winter stratosphere, and depends simply upon the existence of positive vertical shear, or differential rotation, within the vortex. We do so by considering localized wavelike disturbances to a variety of potential vorticity distributions representative of the winter stratosphere.

An interesting theoretical consequence of the preferred downward propagation is that the upper vortex should be stable. In the simulations described below, this is nearly always found to be the case. Even for initially barotropic vortices, which are exceptional, a stable upper vortex is nevertheless established after strong wave breaking there leads to a rounded, dome-like potential vorticity distribution, with the vortex debris forming an annular crown. Such a dome–annulus structure is known to exist in the upper stratosphere, evidence including observations dating to Dunkerton and Delisi (1985) as well as a more recent numerical study of the three-dimensional structure of Rossby wave breaking by Polvani and Saravanan (2000). Although there are many other physical processes certainly at play in the upper stratosphere–lower mesosphere, such as strong diabatic forcing and gravity wave drag, the present framework provides a possible explanation of this structure solely in terms of conservative, balanced dynamics.

The main tool used in the numerical simulations described below is the contour advective semi-Lagrangian model developed originally by Dritschel and Ambaum (1997) and extended to cylindrical geometry by Macaskill et al. (2003). This model is ideal for studying wave motion on a steep-edged polar vortex, such as that observed in the winter stratosphere (Waugh et al. 1994; Plumb et al. 1994). In addition to efficiently capturing the steep potential vorticity gradients of the vortex edge, in a way that gridpoint or pseudospectral models cannot approach, the conservative nature of the model is perfectly suited to the study of wave propagation. Contour displacements allow the easy computation of a nonlinear, conserved wave activity that indicates unambiguously the sense of wave propagation.

Finally, we note that a similar approach was adopted recently by M. Ambaum and J. Methven (2004, personal communication), who considered wave propagation on a polar vortex in the Boussinesq system. Using a similar displacement based measure of wave activity, actually the contour ellipticity, they also demonstrated downward wave propagation from a central disturbance. However, because of the vertical symmetry inherent in the Boussinesq system, upward and downward wave propagation were exactly equal. In contrast, the preference for downward propagation described in this paper and in SD is a direct consequence of the anisotropy associated with the density profile of the compressible atmosphere.

The remainder of the paper is organized as follows. Section 2 summarizes the main ideas of SD that underlie the results presented here. Section 3 contains details of the numerical method used to solve the evolution equations, and a description of the physical parameters and vortex configurations studied in section 4. Section 4 contains the results of a series of numerical calculations of perturbed vortices, and introduces various diagnostics that describe the details of the wave propagation. Section 5 presents our conclusions.

2. Potential vorticity inversion in the compressible case

We first recall some results from SD. The starting point is the quasigeostrophic equations of a polar f plane, written in dimensional form as

$$\frac{Dq}{Dt} \equiv \frac{\partial q}{\partial t} + \mathbf{u} \cdot \nabla q = 0 \tag{1a}$$

$$\nabla_h^2 \psi + \frac{1}{\rho_0} \frac{\partial}{\partial z} \left(\rho_0 \frac{f^2}{N^2} \frac{\partial \psi}{\partial z} \right) = q \tag{1b}$$

$$(u, v) = \left(-\frac{\partial \psi}{\partial y}, \frac{\partial \psi}{\partial x} \right), \tag{1c}$$

where $q(x, y, z, t)$ is the (anomalous) potential vorticity (PV), ψ is the geostrophic streamfunction, $\mathbf{u} = (u, v)$ is the horizontal geostrophic velocity, ρ_0 is the background density, ∇_h^2 is the horizontal Laplacian, x and y are horizontal coordinates, and $z \propto -H \log p$ is an appropriate log-pressure vertical coordinate, with vertical scale height H (cf. Pedlosky 1987). Here, $f = 2\Omega$ is polar value of the Coriolis parameter, where $\Omega = 2\pi$ day^{-1} is the planetary rotation rate, and N is a constant buoyancy frequency. This system is arguably the simplest geophysically relevant model of rotating, stratified flow.

The assumption of constant f and N allows the vertical coordinate z to be rescaled by f/N, rendering the system isotropic in the absence of density variations. When the density is allowed to vary exponentially with height, with $\rho_0 = \rho_s \exp(-z/H)$ where ρ_s is a surface reference density, the situation appropriate to the atmosphere, this isotropy is broken. In that case, nondimensionalizing the horizontal and vertical coordinates by L (a horizontal length scale) and H, respectively, allows Eq. (1b) to be written as

$$\nabla^2\psi - \frac{\partial\psi}{\partial z} = q, \tag{2}$$

where ∇^2 is the usual 3D Laplacian. The effect of the exponential density dependence appears as the second term on the left-hand side.

The underlying result of SD was the derivation of an explicit Green's function solution to Eq. (2). Specifically, the solution to Eq. (2) with the q on the right-hand side replaced by the Dirac delta function $\delta(x, y, z - z')$ takes the form

$$G_\infty(R, z;z') = -\frac{1}{4\pi}\left(\frac{\rho'}{\rho}\right)^{1/2}\frac{e^{-(R/2)}}{R}, \tag{3}$$

where $R \equiv \sqrt{x^2 + y^2 + (z - z')^2}$ is a full 3D radial coordinate from a source point located at $(0, 0, z')$, and where we have used the shorthand notation for the density $\rho = e^{-z}$ and $\rho' = e^{-z'}$.

Directly above and below the source, that is, along the vertical line $r \equiv \sqrt{x^2 + y^2} = 0$, G_∞ reduces to

$$G_\infty(r = 0) = -\frac{1}{4\pi|z - z'|}\begin{cases}1 & \text{for } z > z' \\ \rho'/\rho & \text{for } z > z'\end{cases}, \tag{4}$$

which makes the anisotropy introduced by the compressibility term in Eq. (2) explicit: above the source point z', the Green's function decays algebraically like $1/R$, similar to the Boussinesq limit, whereas below the source the decay is exponential, with a decay scale of one (H in dimensional units). Note that locally, that is, for $R \ll 1$, $G_\infty \approx -1/4\pi R$, which is the form taken by the Boussinesq Green's function.

With this knowledge of the Green's function for the PV inversion operator it is easy to consider the implications of the anisotropy for a vortex of finite volume. Because the streamfunction associated with an element of PV at a particular location decays more slowly above than below, it follows that the upper levels of a finite vortex will spin faster than the lower levels. For spherical vortices in an unbounded domain, SD showed that this differential rotation was greatest when the total vortex depth was around $8H$.

As noted in SD, the picture is complicated by the presence of a lower boundary because of the need to consider the barotropic component otherwise absent in the unbounded domain, but which becomes dominant as the boundary becomes closer to the vortex. The limiting case is that of a columnar vortex spanning the entire domain between an upper and lower boundary, for which the response is purely barotropic. However, for vortices separated from the lower boundary by more than one or two density-scale heights, it turns out that the barotropic contribution is weak compared to the differential rotation.

As can be seen from Fig. 1, the effect of the differential rotation on the nonlinear evolution of an ellipsoidal vortex is dramatic. In the Boussinesq case, a vortex of sufficiently large mean horizontal aspect ratio is unstable to vertically symmetric deformations of the upper and lower vortex. The effect of the instability is to reduce the aspect ratio to a subcritical value. In the compressible case, on the other hand, the vertical symmetry is broken: a similar vortex now experiences rapid deformation in the lower levels, while the upper levels become more circular. This upper stabilization and lower destabilization can be explained entirely in terms of the differential rotation acting together with the strain induced by the ellipticity of the main vortex (see SD for further details).[1]

Finally, it is instructive to consider the above results in the context of recent work by Ambaum and Hoskins (2002), who showed that a PV anomaly of given horizontal scale has different decay scales above and below the anomaly. At first sight, the algebraic decay demonstrated in Eq. (4) may appear in contradiction to their result. However, the vertical decay scales they obtained were a consequence of choosing a priori the horizontal length scale of the response, since this automatically

[1] We use these terms loosely, since in the compressible case the ellipsoidal vortex is not an exact equilibrium solution of the governing equations component and is considerably larger than in the case considered here.

determines the corresponding vertical scale through the vertical structure equation, as described in Waugh and Dritschel (1999). In the present case, there is no preferred horizontal scale because all scales are contained in the delta function response of the Green's function. In fact, Eq. (3) can also be obtained by taking the limit $D \to \infty$ of Waugh and Dritschel's bounded Green's function, that is, an integral over a continuum of vertical modes, each with a different vertical decay scale.

3. Numerical details

To illustrate the effect of the density anisotropy on wave propagation, Eqs. (1) are integrated numerically starting from various initial conditions comprising an axisymmetric vortex plus a wave perturbation. The numerical model used is the contour advective semi-Lagrangian (CASL) model developed originally by Dritschel and Ambaum (1997) and extended to cylindrical geometry by Macaskill et al. (2003). It solves Eqs. (1) in a cylindrical domain using a polar coordinate system (r, θ, z) that rotates about the cylindrical axis $r = 0$ at the rate $\Omega = f/2$, where $f = 4\pi$ corresponds to the polar value of the Coriolis parameter. Lateral boundary conditions are free slip, and isothermal boundary conditions, that is, $\psi_z = 0$, are imposed at the horizontal upper and lower boundaries at $z = 0$ and $z = Z_T$.

Initial conditions are determined by specifying a basic state PV as a function of radial and vertical coordinates r and z together with an azimuthal wavenumber perturbation. The general basic state is defined as

$$q(r, z) = \begin{cases} q_i & r < r_0(z) \\ q_o & r > r_0(z) \end{cases}, \tag{5}$$

where $r_0(z)$ is the mean horizontal vortex radius at a given level, and where q_i and q_o are interior and exterior PV values. We will consider two basic forms of $r_0(z)$. In the first, which gives rise to a spheroidal vortex of vertical aspect ratio c/r_m, $r_0(z)$ satisfies $r_0^2/r_m^2 + (z - z_0)^2/c^2 = 1$. Choosing the maximum horizontal radius $r_m = 3L_R$, where $L_R = NH/f$ is the Rossby deformation radius, $c = 4H$, and centroid $z_0 = 6H$, produces a vortex whose vertical and horizontal extent corresponds roughly to that of the stratospheric polar vortex.

The second form of $r_0(z)$, and that used in most of the simulations below, corresponds to a columnar vortex, truncated above and below specified levels, z_t and z_b, respectively. Specifically,

$$r_0(z) = \begin{cases} r_m & z_b < z < z_t \\ 0 & \text{otherwise} \end{cases}. \tag{6}$$

Again, choosing the horizontal radius $r_m = 3L_R$ with $z_b = 2H$ and $z_t = 10H$ corresponds roughly to the dimensions of the stratospheric polar vortex. The special case $z_b = 0$, $z_t = Z_T$ corresponds to a barotropic vortex such as that considered by Dritschel and Saravanan (1994, hereafter DS94).

Having defined the basic state vortex, an azimuthal perturbation is added by deforming the vortex boundary with a disturbance of azimuthal wavenumber $m = 1, 2, 3 \ldots$. In polar coordinates, the vortex boundary is displaced from $r = r_0(z)$ to

$$r(\theta, z) = \alpha(z)[r_0(z) + \eta(z) \cos m\theta], \tag{7}$$

where the disturbance amplitude $\eta(z)$ has a Gaussian form, given by

$$\eta(z) = \eta_{\max} e^{-\left(\frac{z - z_m}{H}\right)^2}, \tag{8}$$

where $\eta_{\max}$ is the maximum disturbance amplitude and where the height of the disturbance $z_m = 6H$ is chosen to be at the midlevel of the domain. In Eq. (7) the normalization factor $\alpha(z) = r_0^2/(r_0^2 + \frac{1}{2}\eta(z)^2)$ is chosen to ensure that the areas enclosed within each horizontal cross section of the vortex are equal, that is, so that the disturbance is area preserving.

The equations are discretized using 120 layers in the vertical between $z = 0$ and $z = Z_T = 12H$, where the vertical scale height, $H = 6146$ m is representative of the stratosphere. Notionally, the vertical domain extends from the ground to near the top of the mesosphere. In the horizontal, the streamfunction and velocity fields are calculated on a stretched grid of 128 radial and 264 azimuthal points, although the PV itself is first interpolated onto a grid 4 times finer for more accurate inversion. The stretched grid concentrates radial grid points near the pole, distributing them uniformly in $r^{1/2}$ for improved resolution in the region of interest (providing about 42 radial grid points between the origin and a vortex edge at $r_m = 3L_R$). The lateral boundary is located at a distance of $30L_R$, or 10 vortex radii, from the pole, far away to have practically no effect on the evolution. The solutions calculated at this resolution and in this domain size are numerically converged, in the sense that increasing the resolution or domain size further has no visible effect on any of the results.

4. Results

In general, a localized perturbation of the form Eq. (7) will propagate away from its initial location as a vertically propagating Rossby wave. In the Boussinesq system, in which the background density is constant with height, there is no preferred direction and waves

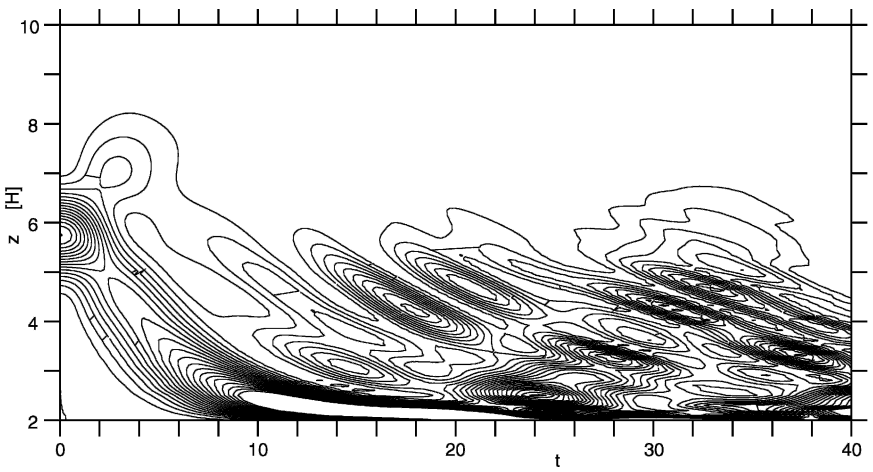

FIG. 2. Wave activity as a function of height and time on a spheroidal vortex (case $\mathcal{S}$), of vertical extent $D \equiv 2c = 8H$ and vertical aspect ratio $c/r_m = 4/3$, with a wavenumber-2 perturbation of amplitude $\eta_{\max} = 0.2r_m$ in the central levels.

will propagate equally upward and downward. The background density variation present in the compressible system breaks that symmetry.

As was shown in SD (and Fig. 1), for the case of perfect ellipsoidal vortices, the effect of the compressibility is to induce a differential rotation that stabilizes the upper vortex and destabilizes the lower vortex. The ellipsoids in that study can be regarded as spheroidal vortices plus an approximate wavenumber-2 perturbation throughout the whole vortex depth. Although that study showed a clear accumulation of wave activity in the lower vortex, it is difficult to consider cleanly the precise details of wave propagation, because modal disturbances on the scale of the ellipsoids are excited and propagate in all directions. In the present paper, the localization of the initial disturbance [Eq. (8)] removes this drawback and allows a cleaner examination of the precise details of the wave propagation.

a. Spheroidal vortex

As a first point of departure from SD, we consider the case of a spheroidal vortex, of vertical aspect ratio $c/r_m = 4/3$, half-height $c = 4H$, maximum horizontal radius $r_m = 3L_R$ centered at $z_0 = 6H$; this case is labeled $\mathcal{S}$ below. Interior and exterior PV values are chosen to be $q_i = 1.3$ and $q_o = 0.9$, following Dritschel and Saravanan (1994), although this will be modified in many of the cases below. The initial azimuthal perturbation has an $m = 2$ wavenumber and an amplitude of $\eta_{\max} = 0.2r_m$.

As a principle diagnostic we will consider the wave activity A, defined as the departure from circularity of a contour on a given level by

$$A(z, t) = \rho_0(z)q \oint_{\Gamma(z)} [Y(\theta, z, t) - Y_e(z)]^2 d\theta, \qquad (9)$$

where the integral is taken around a closed contour Γ at height z, θ is an azimuthal coordinate, $Y = \frac{1}{2}r^2$ (so that $dY\, d\theta$ is the differential area), $Y_e = \frac{1}{2}r_e^2$, and where r_e is the radius of the undisturbed circular contour enclosing the same area as Γ. As defined, A is a nonlinear pseudomomentum based wave activity, second order in disturbance amplitude, which satisfies an exact conservation relation [see Dritschel (1988) and Dritschel and Saravanan (1994) for more details].

Figure 2 shows the wave activity as a function of height within the vortex (there can be no wave activity above or below the vertical extent of the vortex) and time in days for case $\mathcal{S}$. The initial wave disturbance can be seen localized at $z = 6H$ at time $t = 0$. As time increases, there is a clear downward preference to the wave propagation. Although there is also a small upward contribution, this is overwhelmingly dominated by the downward propagation. The downward propagation continues all the way down the vortex slowing slightly as it approaches the lowermost levels, with the wave activity increasing as it is confined into a smaller vertical region. Note that the vertical integral of A is conserved in time in the absence of dissipation, which at these early times is negligible. At later times, long after the initial downward propagation of the disturbance, weaker events are identifiable when wave activity is refocused into a particular region (presumably from lower levels, although this is difficult to identify precisely). Again, the downward propagation of these subsequent disturbances is clear.

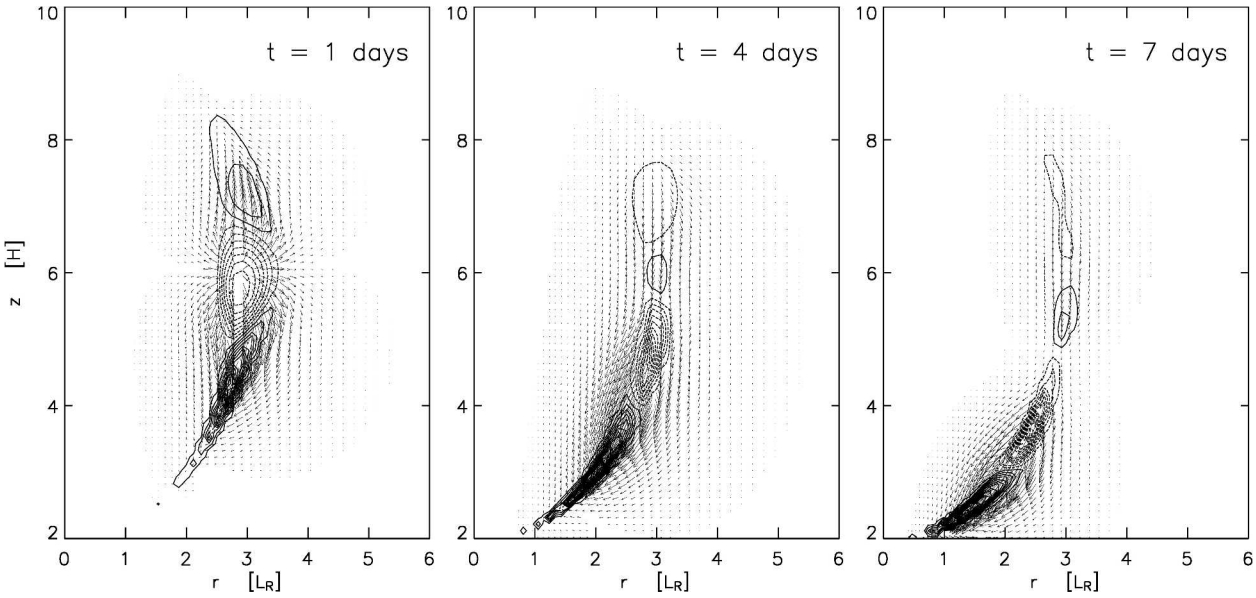

FIG. 3. The EP fluxes and convergence for the case shown in Fig. 2 (case $\mathcal{S}$) at times $t = 1$ day, $t = 4$ days, and $t = 7$ days. Graphical conventions follow Dunkerton et al. (1981) with appropriate modifications for cylindrical geometry. Note that the true EP fluxes are presented, with no density rescaling, as these are the relevant measure of wave propagation.

Another, closely related, measure of wave propagation is the Eliassen–Palm (EP) flux described in Andrews and McIntyre (1978). For the quasigeostrophic system, this takes the form given in Andrews et al. [1987, Eq. (3.5.6)]. Note that the diagnostic used here is the true EP flux, a true measure of the flux of wave activity A, rather than the frequently shown EP flux normalized by the density, which emphasizes wave motions in the upper atmosphere but is not a meaningful, conservative measure of wave activity.

Figure 3 shows snapshots of the EP flux and its convergence at $t = 1$, $t = 4$, and $t = 7$ days in the height-radial plane. At $t = 1$ day, wave activity can be seen to radiate upward and downward away from the central perturbed region near $z_0 = 6H$. Already at this time it is clear that the downward propagation is considerably stronger than the upward propagation. As time progresses, the downward propagating region continues steadily downward. On the other hand, the initial weak burst of upward propagation soon reverses and can be seen to be propagating downward again by $t = 4$ and $t = 7$ days. It is visible in Fig. 2 as the weak downward tilting region of wave activity that begins in the middle of the domain around $t = 6$ days. This reversal is consistent with properties of wave propagation on a slowly varying (in the vertical) background state derived using Wentzel–Kramers–Brillouin (WKB) techniques. In particular, a variant of the quasigeostrophic refractive index (Harnik and Lindzen 2001) predicts that vertically propagating waves will be reflected downward by negative shear in the upper stratosphere, as they are found to do here.

Two final points are worth observing. First, because waves are confined to the vortex edge, that is, where there is a nonzero gradient of PV, the EP flux and convergence are similarly confined. Indeed the vortex edge can be clearly made out in Fig. 3. Second, because the initial perturbation and hence wave amplitudes are fairly weak in this case, the flow is essentially dissipationless, with no wave breaking or filamentation of the vortex edge. Therefore, according to the nonacceleration theorem (Charney and Drazin 1961; Andrews and McIntyre 1978), all the flux convergence seen in Fig. 3 can be attributed purely to wave transience: as the wave packet enters a region the convergence is positive and as it leaves again the convergence is negative. At later times, filamentation occurs and dissipation becomes more important. The trapping of wave activity in lower levels may be associated with critical layer effects in this region. Although the precise location of such a layer is difficult to establish because of the complicated space and time dependence of the disturbance phase speed, a rough estimate indicates that a critical layer may exist near the lowermost vortex levels.

b. Columnar vortex

The spheroidal vortex considered above could be regarded as a somewhat peculiar idealization of the stratospheric polar vortex because its surface closes

smoothly at each end. For example, it is conceivable that the curvature of the vortex shape might give a preference for downward propagation simply through a focusing of wave activity, perhaps enhanced somehow by the background density variation. To address this issue, the above experiment was repeated using a columnar vortex profile, similar to that used in previous studies of wave breaking on a simple vortex edge (e.g., Dritschel and Saravanan 1994; Polvani and Saravanan 2000; Scott et al. 2004).

The simplest comparison is for a columnar vortex of the same maximum vertical and horizontal extent as $\mathcal{S}$, that is, $c = 4$ and $r_m = 3L_R$, using Eq. (6) to define the vortex edge and keeping the same values of $q_i = 1.3$ and $q_o = 0.9$. For these values of q_i and q_o, however, it turns out that the zonal mean zonal velocity field associated with the vortex is unrealistically weak, with a jet maximum around only 30 m s^{-1}. The reason why identical values of q_i and q_o give rise to a much weaker vortex here than in DS94 (where the jet maximum was close to 60 m s^{-1}) is that here the vortex is truncated at $z = 2H$ and does not extend all the way to the ground. As was shown in SD, the effect of a lower boundary close to a PV source is the introduction of a large barotropic component, and in the case of DS94, this barotropic component is considerably larger than in the case considered here.

It turns out, therefore, that to achieve a realistically strong jet maximum in a vortex of the above vertical extent, it is necessary to increase the values of q_i and q_o. Note, however, that because the evolution is insensitive to an arbitrary background rotation, the effect of these parameters is only felt through the PV jump $\Delta q = q_i - q_o$. Furthermore, as can be seen from Eqs. (1), the only effect of changing Δq is a change in the time scale of the system. Thus, increasing Δq increases the jet maximum and decreases the time scale of the nonlinear evolution, so the vortex evolves on a shorter time scale but otherwise identically as before.

Without loss of generality, therefore, we consider the columnar case with $q_i = 1.5$ and $q_o = 0.95$, labeled $\mathcal{C}$ below. The zonal mean zonal velocity $\bar{u}$ for the spheroidal case $\mathcal{S}$ and for the columnar case $\mathcal{C}$ is shown in Figs. 4a,b. At first sight, it appears that the shape of $\mathcal{C}$ is more representative of the winter stratosphere than that of $\mathcal{S}$ with a stronger jet maximum of around 60 m s^{-1} and a zero wind line at more realistic lower latitudes. It should be remembered, however, that these features could also have been achieved for $\mathcal{S}$ by suitable choices of q_i and q_o. A fairer comparison would therefore be obtained by visualizing the (bold) zero wind line in Fig. 4a shifted three contours to the right.

Figure 5 shows the evolution of the wave activity for case $\mathcal{C}$. Again the dominance of the downward propagation is immediately clear, and indicates that the phenomenon is not simply due to the special geometry of the spheroidal vortex. As described above, the evolution for the same case but with $q_i = 1.3$ and $q_o = 0.9$ is identical, except that the downward propagation occurs over a slightly longer time scale.

Figure 6 shows the EP fluxes for case $\mathcal{C}$ at times $t = 1$, $t = 4$, and $t = 7$ days. Again, at time $t = 1$ the downward propagation from the initial disturbance is dominant. As for case $\mathcal{S}$ above, the initial upward burst is seen to partially reverse in the upper vortex and begin propagating downward by $t = 4$, contributing to the appearance of the secondary downward propagation event seen in Fig. 5 around $t = 4$. Again, the reversal is consistent with wave reflection in the upper vortex.

c. Dependence on disturbance amplitudes

The above results were obtained with a disturbance amplitude of $\eta = 0.2r_m$, which is a relativity small disturbance. In fact, simulations with smaller amplitude (not shown) produced very similar results, with only a slight flattening of the slope of downward propagation, indicating that the above wave propagation is in a nearly linear regime.

An interesting question is what is the nature of the response to much larger disturbances, when nonlinearity can be expected to play an important role. To test this, case $\mathcal{C}$ was repeated using a disturbance amplitude of $\eta = r_m$. For this value, the initial disturbance on the central level is such that the middle vortex contour pinches in two, forming a figure-eight horizontal cross section. Such a symmetric pinching of the vortex is similar to that often observed in the early stages of wave-2 dominated major stratospheric warming events (e.g., McIntyre and Palmer 1983), and similar to that observed in the recent Southern Hemisphere major warming event of 2002 [e.g., Newman and Nash (2005), and the special issue of the *Journal of Atmospheric Sciences* (2005, vol. 62, no. 3) on the 2002 Southern Hemisphere warming and ozone split].

Because of the magnitude of this disturbance, the nonlinear evolution is dominated by the intense distortion and filamentation of the central vortex, with much vortex material thrown off the main column. As can be seen from Fig. 7, these vortex remnants contain a large fraction of the initial wave activity, which persists at midlevels, gradually decreasing as the debris is eroded by the contour surgery. In addition to this midlevel wave activity, however, there is again a clear component of downward propagation and an accumulation of wave activity in the lowermost levels of the vortex.

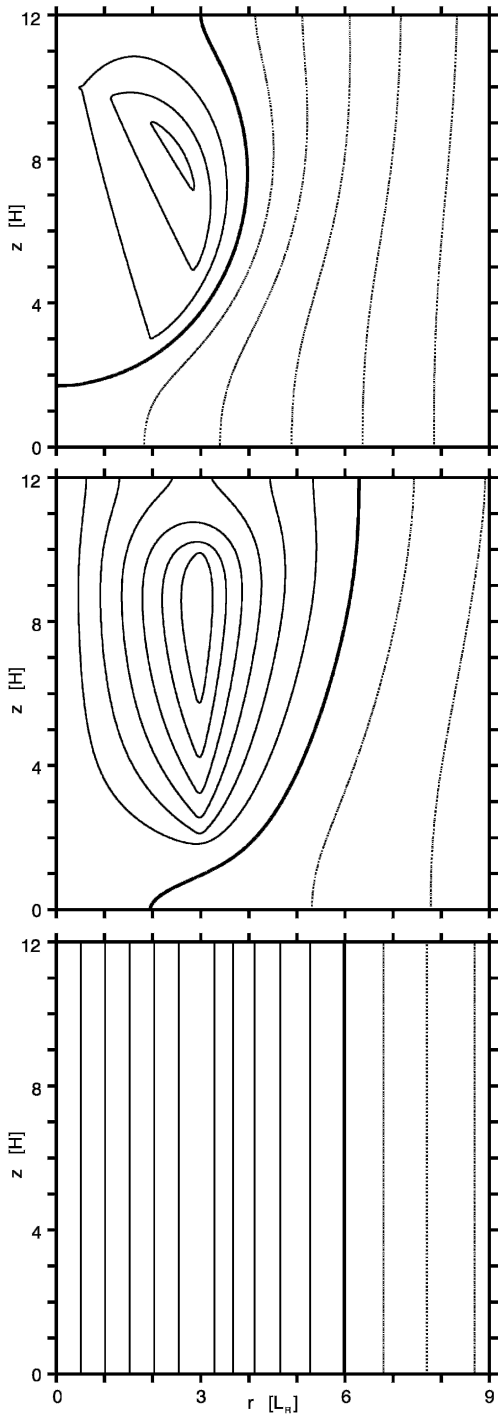

FIG. 4. Initial zonal mean zonal velocity, $\overline{u}(t = 0)$, corresponding to different PV distributions: (a) case $\mathcal{S}$, a spheroid with a uniform background rotation (corresponding to interior and exterior PV values of $q_i = 1.3$ and $q_o = 0.9$); (b) case $\mathcal{S}$, a column of vertical extent $D = 8H$ with $q_i = 1.5$ and $q_o = 0.95$; (c) case $\mathcal{BT}$, a column of vertical extent $D = 12H$ with $q_i = 1.3$ and $q_o = 0.9$. Contour interval is 10 m s^{-1}; positive, negative, and zero values are contoured using solid, dotted, and bold lines, respectively.

d. Importance of vertical shear

As discussed in SD, it is the existence of vertical shear, or differential rotation, that is responsible for the stabilization of the upper vortex and destabilization of the lower vortex, and which gives rise to the preference for downward propagation shown above. As a further illustration of the importance of vertical shear, we consider next the evolution of a disturbance on a purely barotropic vortex. For this, we choose $q_i = 1.3$ and $q_o = 0.9$ following DS94, and set $z_b = 0$ and $z_t = 12$, so that the vortex spans the entire vertical domain. The zonal mean velocity is shown in Fig. 4c for easy comparison with case $\mathcal{C}$. Note that this barotropic velocity profile is identical to that of DS94. We label this case as $\mathcal{BT}$ in what follows.

Figure 8 shows the evolution of the wave activity for $\mathcal{BT}$. Now, the initial disturbance gives rise to equally strong upward and downward propagating waves, with the initial wave activity remaining approximately symmetric about $z = 6H$ at early times. In particular, there is no trace of preferential downward propagation. The symmetry is broken at later times as nonlinearities, particularly in the upper vortex, lead to filamentation and dissipation of the wave activity.

It is worth noting that the purely barotropic structure of the vortex $\mathcal{BT}$ arises because the PV distribution spans the entire vertical domain. However, a largely barotropic response will be found for any distribution concentrated near the lower boundary, a consequence of the bounded Green's function described in Waugh and Dritschel (1999) and SD. In actual atmospheric flows, however, the PV in the troposphere is in general weaker than that in the stratosphere (under the appropriate vertical scaling) and, as a consequence, the vertical structure of the zonal velocity is closer to that of case $\mathcal{C}$ than that of $\mathcal{BT}$ (see Figs. 4b,c). In general, one observes significant positive vertical shear in the upper troposphere and lower to middle stratosphere, and so one should expect the conditions for preferential downward propagation to be satisfied. For this reason, we should also be careful when interpreting the results of idealized studies of wave propagation on barotropic vortices.

The upward propagation on the vortex $\mathcal{BT}$ has an interesting impact on the upper vortex PV structure. The strong filamentation of the upper vortex erodes the initially columnar form to produce a smoother dome-like shape at later times, surrounded by an annulus of filamentary PV debris. The evolution of the vortex itself is shown in Fig. 9 at times $t = 0$, 5, 10, 15, 20, and 40 days. The initial perturbation is visible at time $t = 0$ and is seen to propagate upward and eventually leads to

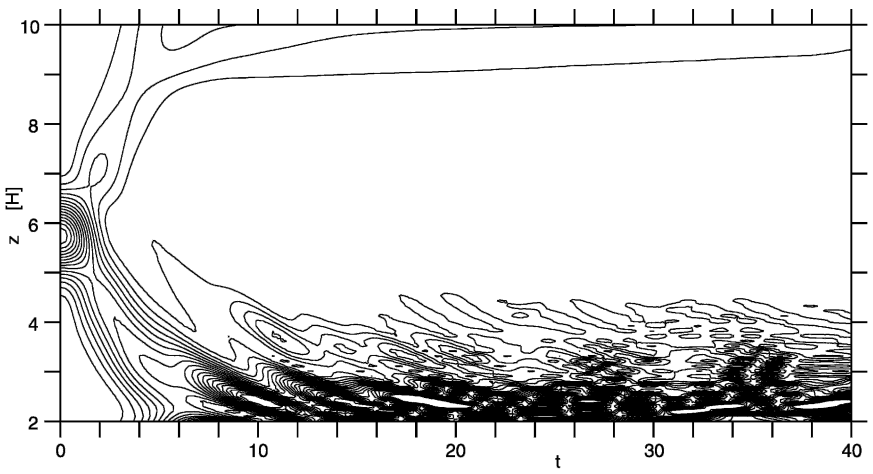

FIG. 5. Wave activity as a function of height and time for the columnar case *C* with a perturbation of amplitude $\eta_{\max} = 0.2r_m$ in the central levels.

strong nonlinear distortion of the upper vortex. Note that, although the wave activity is propagating symmetrically upward and downward (Fig. 8), contour displacements in the upper vortex are much larger than those in the lower vortex on account of the smaller mass of the former. By $t = 20$ the dome shape and surrounding annulus is clearly visible.

Because the cross-sectional area of the upper vortex at later times decreases with height, there arises a positive vertical shear at a given location within the vortex, with the upper vortex rotating faster than that at lower levels. In other words, a stabilizing differential rotation is established in the upper vortex, as can be seen from Fig. 10, which shows the angular velocity at $t = 0$ and $t = 40$. Because of this differential rotation, the dome-like shape is robust (cf. with the spheroidal vortex) and it again produces a preference for downward wave propagation. The upper vortex has thus moved from a state in which upward wave propagation and vortex distortion was easy, to a more stable one in which it is inhibited.

e. Other wavenumber disturbances

The mechanism described in SD, whereby the faster spinning upper vortex is stabilized and the slower spin-

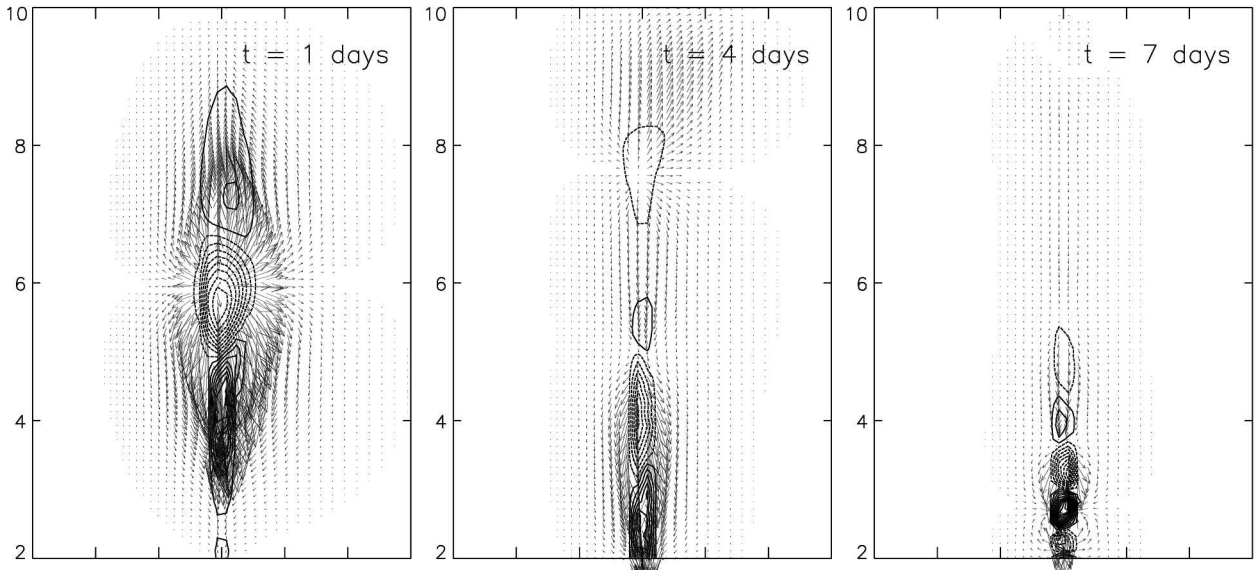

FIG. 6. As Fig. 3 but for the columnar case *C*.

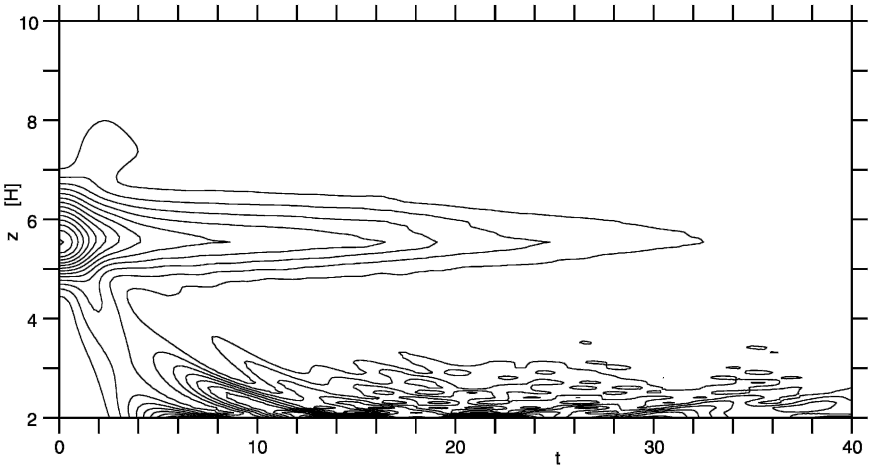

FIG. 7. Wave activity as a function of height and time for case $\mathcal{C}$ with a wavenumber-2 perturbation of amplitude $\eta_{\max} = r_m$.

ning lower vortex is destabilized, relied on the horizontal elliptical form of the disturbance. It was the orientation of the upper and lower elliptical cross sections to the straining flow induced by the main vortex that determined whether these upper and lower contours would be squashed back to circularity or to greater eccentricity. One might well ask, therefore, whether the above preference for downward propagation relies also on the fact the initial central disturbance has a wave-2 form, this being, at least for small amplitudes, largely elliptical.

To answer this question, case $\mathcal{C}$ above was repeated with initial disturbances of different azimuthal wavenumbers, as determined by the parameter m in Eq. (7). Figure 11 shows the evolution of the wave activity on vortices identical to $\mathcal{C}$ but with initial disturbances of wavenumber $m = 1$ (upper panel) and $m = 3$ (lower panel). As is evident, in each case most of the initial

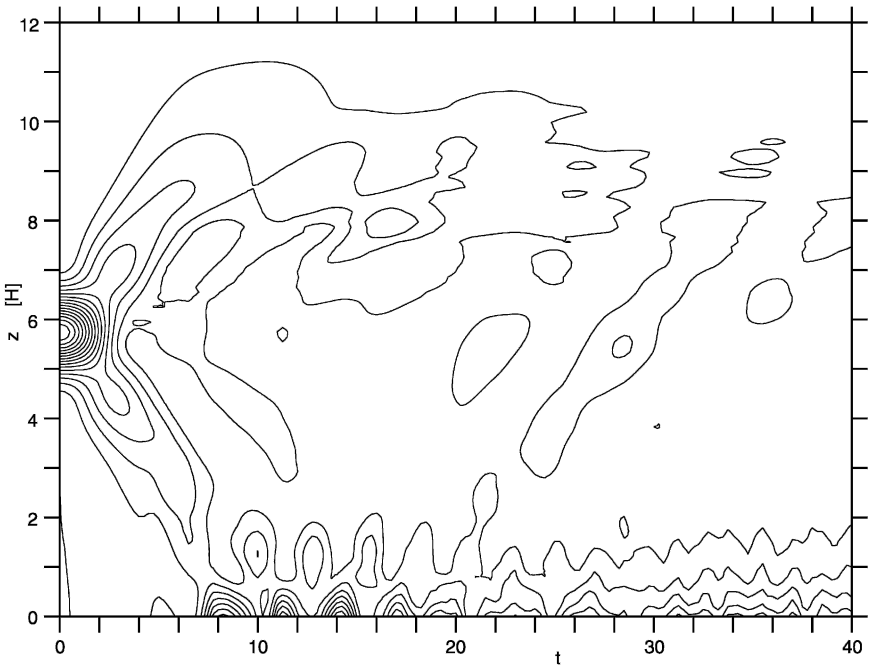

FIG. 8. Wave activity as a function of height and time for case $\mathcal{BT}$ with a wavenumber-2 perturbation of amplitude $\eta_{\max} = 0.2r_m$.

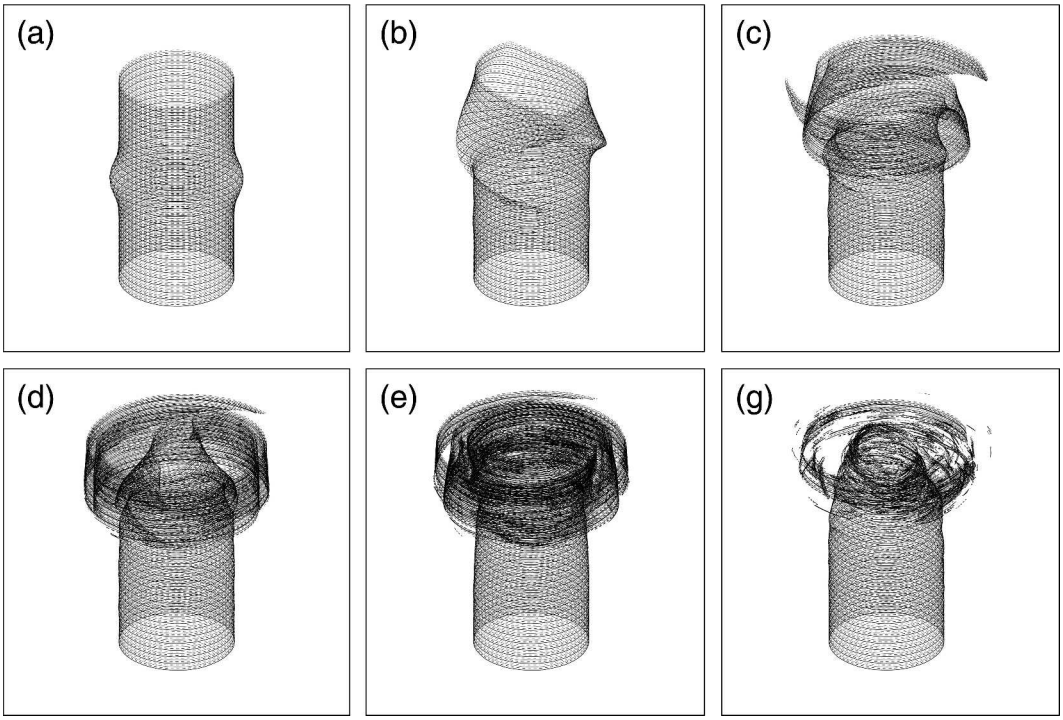

FIG. 9. Vortex structure for case $\mathcal{BT}$ at times (a) $t = 0$ days, (b) $t = 5$ days, (c) $t = 10$ days, (d) $t = 15$ days, (e) $t = 20$ days, and (f) $t = 40$ days.

wave activity again propagates downward, accumulating in the lower levels. A closer inspection reveals some differences. For example, the initial asymmetry is stronger for higher m (see also Fig. 5 for the case $m = 2$), the ratio of downward to upward propagating wave activity begin slightly less than double for $m = 1$, but well over triple for $m = 3$. However, as time progresses, it can be seen that some of the initially upward propagating wave activity in the case $m = 1$ is reflected downward again around $t = 8$. The same happens with $m = 3$ but to a lesser extent and earlier. Similarly, there is more evidence of repeated downward propagation events at much later times for $m = 1$, presumably because in that case there is a larger reservoir of wave activity distributed throughout the upper vortex as a result of the larger initial upward pulse. The key point to note, however, is that, despite the nonellipticity of the initial disturbances, there is still a strong preference for the downward propagation of these azimuthal wavenumbers. This can perhaps be best understood by a comparison with the phase properties of vertically propagating waves. As before, the vertical shear causes the disturbance at upper levels to be shifted eastward relative to the disturbance at lower levels. This shift is nothing but an eastward phase tilt with height and is therefore associated with a downward group velocity of the disturbance.

5. Discussion

We have seen that a wavelike disturbance placed in the central levels of an ellipsoidal or columnar vortex propagates predominantly downward away from the initial disturbance region, roughly twice as much wave activity going downward as upward. The predominance is less for lower wavenumber disturbances than for higher, but is still significant even for wavenumber 1. The effect is clearly visible both in the wave activity based on contour displacements, and in the traditional EP fluxes calculated from the full velocity and streamfunction fields. Although we have considered very simple vortex configurations, our results appear robust. One avenue for future work, however, would be to consider wave propagation on more realistic vortex distributions.

The preference for downward propagation arises from the presence of vertical shear, or differential rotation, within the vortex, which is itself a consequence of the anisotropy introduced into the Green's function by the exponential profile of the background density. Because a disturbance in the upper vortex is rotating faster than that on the central vortex below, its phase is advanced relative to the induced velocity anomaly of the central disturbance below. This phase advance is such that the velocity anomaly reduces the upper dis-

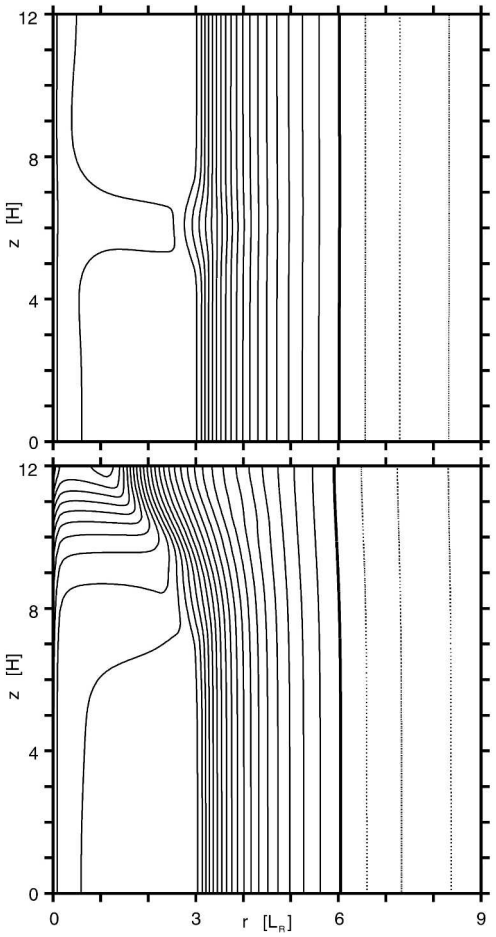

FIG. 10. Angular velocity for case $\mathcal{BT}$ at times (top) $t = 0$ days and (bottom) $t = 40$ days. Positive, negative, and zero values are contoured using solid, dotted, and bold lines, respectively.

turbance, squashing it back to circularity. Similarly, a disturbance on the lower vortex is rotating slower than that on the central above, its phase is retarded, and the velocity anomaly amplifies the lower disturbance further. Thus, the faster rotating upper vortex is stabilized, whereas the slower rotating lower vortex is destabilized (see SD for details). An alternative view is that the vertical shear gives rise to an eastward phase tilt of the disturbance with height, which is associated with a downward group velocity.

The fact that vertical shear is necessary to produce this effect was demonstrated using a purely barotropic, columnar vortex. In that case, the absence of vertical shear allowed the waves to propagate equally upward and downward away from the disturbance. It should be emphasized, however, that this is a very special case, whose relevance to the stratosphere is limited. In particular, when the PV in the lower levels is weak, as it is in the troposphere, such a strong barotropic response is absent and vertical shear occurs naturally. Such is the case in the atmosphere, where strong vertical shear exists throughout the troposphere and stratosphere, the stratospheric jet generally peaking toward the stratopause. An interesting area for future research lies in the possibility of detecting such preferential downward propagation in observed stratospheric flows. Wave diagnostics of the form used above that can be applied directly to observed fields are currently being developed by the authors for this purpose.

One consequence of the above is the stabilization under general circumstances of the upper vortex. In the case when the initial flow has no vertical shear, as in case $\mathcal{BT}$ above, upward wave propagation causes strong wave breaking in the upper vortex, with filamention and the reduction of the cross-sectional area in upper levels. The result is the formation of a domelike configuration in which the vortex area decreases with height. This formation has been observed in many model simulations, including those presented here as well as in previous studies (e.g., Polvani and Saravanan 2000; Scott et al. 2004), and appears to be a robust feature. As the domelike formation forms, the vortex moves toward a more stable distribution, similar to the spheroid, with positive differential rotation, thereby inhibiting further vortex destruction.

In addition to the formation of a domelike configuration, the wave breaking on the upper vortex also gives rise to an annular ring of high PV consisting of filamentary debris (Fig. 9). In the calculation here, in which contour surgery gradually removes finescale structures, this debris diminishes gradually in the absence of further wave breaking to replenish it. One could speculate, however, that in a forced dissipative system, in which the upper vortex was radiatively forced toward a stronger configuration, persistent wave breaking could act as a continuous source for this filamentary debris. In that scenario, a balance would arise between the removal of the debris by dissipation and the creation of more debris by wave breaking, and a persistent annulus structure would emerge. Such a structure has been known to exist in the mesosphere since the early observations of Dunkerton and Delisi (1985). Of course, it is naive to apply concepts of conservative, balanced dynamics to a region of the atmosphere where gravity wave drag and strong radiative effects are capable of producing large accelerations. These physical effects almost certainly play a major role in determining the mesospheric PV distribution. Nonetheless, it is interesting to observe that the simple mechanism described here also gives rise naturally to the same type of distribution.

Lastly, it may have been noticed that no discussion

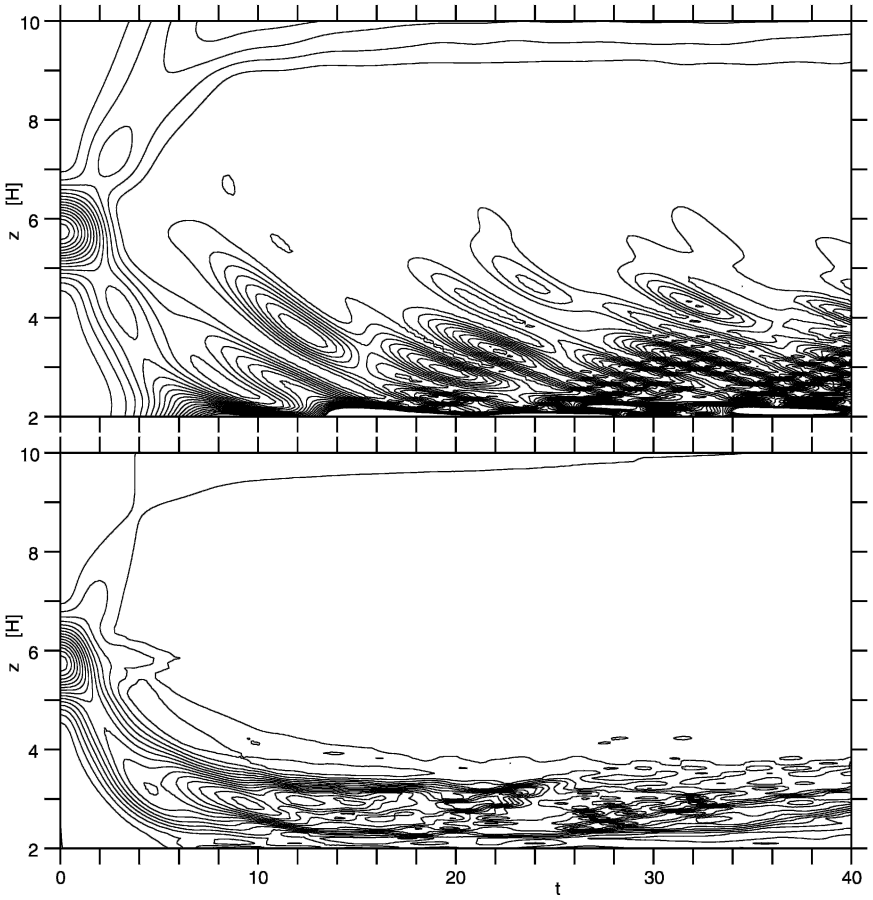

FIG. 11. As in Fig. 5, but with a perturbation of amplitude $\eta_{\max} = 0.2r_m$ of (top) wavenumber 1 and (bottom) wavenumber 3.

has been given to the physical justification for disturbing the vortex in its central levels. One answer to this is that we are simply interested in whether waves propagate upward or downward, and so a central disturbance is natural, and no discussion need be given of how it might arise in reality. However, one might nevertheless speculate about the origin of actual disturbances in the interior of the stratosphere. One origin, for example, could be downward propagation from disturbances higher up, such as the mesospheric 2-day wave. However, because the wave activity is proportional to the vortex displacement times the density, the amount of wave activity in such an upper atmospheric disturbance is almost certainly much too small to be of significance in the lower stratosphere.

The alternative, of course, is wave excitation from below. In the traditional view, waves are generated in the troposphere and propagate up on the polar vortex edge. When wave amplitudes become large, however, and nonlinear effects become important, the notion of upward propagation ceases to be appropriate. For example, during a major stratospheric warming, the entire vortex is violently distorted, or even destroyed completely at certain levels, and further upward propagation is prevented. One may then think of an in situ disturbance at a given level, which may subsequently propagate up or down. This scenario is similar to the case presented in Fig. 7, in which the vortex in central levels is split as in a wave-2 major warming. What these results indicate is that there may be significant downward wave propagation following such events.

Acknowledgments. We are grateful to Tim Dunkerton, Gavin Esler, and Nili Harnik for helpful discussions and to Maarten Ambaum and John Methven for sharing unpublished results. Support for this research was provided by the U.K. Natural Environment Research Council under Grant NER/B/S/2002/00567.

REFERENCES

Ambaum, M. H. P., and B. J. Hoskins, 2002: The NAO troposphere–stratosphere connection. *J. Climate,* **15,** 1969–1978.

Andrews, D. G., and M. E. McIntyre, 1978: Generalized Eliassen–Palm and Charney–Drazin theorems for waves on axisymmetric flows in compressible atmospheres. *J. Atmos. Sci.,* **35,** 175–185.

——, J. R. Holton, and C. B. Leovy, 1987: *Middle Atmosphere Dynamics.* Academic Press, 489 pp.

Baldwin, M. P., and T. J. Dunkerton, 1999: Downward propagation of the Arctic Oscillation from the stratosphere to the troposphere. *J. Geophys. Res.,* **104,** 30 937–30 946.

——, and ——, 2001: Stratospheric harbingers of anomalous weather regimes. *Science,* **294,** 581–584.

Charney, J. G., and P. G. Drazin, 1961: Propagation of planetary-scale disturbances from the lower into the upper atmosphere. *J. Geophys. Res.,* **66,** 83–109.

Dritschel, D. G., 1988: Nonlinear stability bounds for inviscid, two-dimensional, parallel or circular flows with monotonic vorticity, and the analogous three-dimensional quasi-geostrophic flows. *J. Fluid Mech.,* **191,** 575–582.

——, and R. Saravanan, 1994: Three-dimensional quasi-geostrophic contour dynamics, with an application to stratospheric vortex dynamics. *Quart. J. Roy. Meteor. Soc.,* **120,** 1267–1297.

——, and M. H. P. Ambaum, 1997: A contour–advective semi-Lagrangian numerical algorithm for simulating fine-scale conservative dynamical fields. *Quart. J. Roy. Meteor. Soc.,* **123,** 1097–1130.

Dunkerton, T. J., and D. P. Delisi, 1985: The subtropical mesospheric jet observed by the Nimbus 7 limb infrared monitor of the stratosphere. *J. Geophys. Res.,* **90D,** 10 681–10 692.

——, C.-P. F. Hsu, and M. E. McIntyre, 1981: Some Eulerian and Lagrangian diagnostics for a model stratospheric warming. *J. Atmos. Sci.,* **38,** 819–843.

Harnik, N., and R. S. Lindzen, 2001: The effect of reflecting surfaces on the vertical structure and variability of stratospheric planetary waves. *J. Atmos. Sci.,* **58,** 2872–2894.

Holton, J. R., P. H. Haynes, M. E. McIntyre, A. R. Douglass, R. B. Rood, and L. Pfister, 1995: Stratosphere–troposphere exchange. *Rev. Geophys.,* **33,** 403–439.

Macaskill, C., W. E. P. Padden, and D. G. Dritschel, 2003: The CASL algorithm for quasi-geostrophic flow in a cylinder. *J. Comput. Phys.,* **188,** 232–251.

McIntyre, M. E., 1990: Middle atmospheric dynamics and transport: Some current challenges to our understanding. *Dynamics, Transport and Photochemistry in the Middle Atmosphere of the Southern Hemisphere: San Francisco NATO Workshop,* A. O'Neill, Ed., Kluwer, 1–18.

——, and T. N. Palmer, 1983: Breaking planetary waves in the stratosphere. *Nature,* **305,** 593–600.

Newman, P. A., and E. R. Nash, 2005: The unusual Southern Hemisphere stratosphere winter of 2002. *J. Atmos. Sci.,* **62,** 614–628.

Pedlosky, J., 1987: *Geophysical Fluid Dynamics.* 2d ed. Springer-Verlag, 710 pp.

Perlwitz, J., and N. Harnik, 2003: Observational evidence of a stratospheric influence on the troposphere by planetary wave reflection. *J. Climate,* **16,** 3011–3026.

Plumb, R. A., and Coauthors, 1994: Intrusions into the lower stratospheric Arctic vortex during the winter of 1991–92. *J. Geophys. Res.,* **99,** 1089–1105.

Polvani, L. M., and R. Saravanan, 2000: The three-dimensional structure of breaking Rossby waves in the polar wintertime stratosphere. *J. Atmos. Sci.,* **57,** 3663–3685.

Scott, R. K., and D. G. Dritschel, 2005: Quasi-geostrophic vortices in compressible atmospheres. *J. Fluid Mech.,* **530,** 305–325.

——, ——, L. M. Polvani, and D. W. Waugh, 2004: Enhancement of Rossby wave breaking by steep potential vorticity gradients in the winter stratosphere. *J. Atmos. Sci.,* **61,** 904–918.

Thompson, D. W. J., and J. M. Wallace, 1998: The Arctic Oscillation signature in the wintertime geopotential height and temperature fields. *Geophys. Res. Lett.,* **25,** 1297–1300.

——, M. P. Baldwin, and J. M. Wallace, 2002: Stratospheric connection to Northern Hemisphere wintertime weather: Implications for prediction. *J. Climate,* **15,** 1421–1428.

Waugh, D. W., and D. G. Dritschel, 1999: The dependence of Rossby wave breaking on the vertical structure of the polar vortex. *J. Atmos. Sci.,* **56,** 2359–2375.

——, and Coauthors, 1994: Transport of material out of the stratospheric Arctic vortex by Rossby wave breaking. *J. Geophys. Res.,* **99,** 1071–1088.